Nanoenzymology of the 20S Proteasome: Proteasomal Actions Are Controlled by the Allosteric Transition[†]

Pawel A. Osmulski and Maria Gaczynska*

Institute of Biotechnology, University of Texas Health Science Center at San Antonio, 15355 Lambda Drive, San Antonio, Texas 78245

ABSTRACT: The proteasome is a major cytosolic proteolytic assembly, essential for the physiology of eukaryotic cells. Both the architecture and enzymatic properties of the 20S proteasome are relatively well understood. However, despite longstanding interest, the integration of structural and functional properties of the proteasome into a coherent model explaining the mechanism of its enzymatic actions has been difficult. Recently, we used tapping mode atomic force microscopy (AFM) in liquid to demonstrate that the α-rings of the proteasome imaged in a top-view position repeatedly switched between their open and closed conformations, apparently to control access to the central channel. Here, we show with AFM that the molecules in a side-view position acquired two stable conformations. The overall shapes of the 20S particles were classified as either barrel-like or cylinder-like. The relative abundance of the two conformers depended on the nature of their interactions with ligands. Similarly to the closed molecules in top view, the barrels predominated in control or inhibited molecules. The cylinders and open molecules prevailed when the proteasome was observed in the presence of peptide substrates. Based on these data, we developed the two-state model of allosteric transitions to explain the dynamics of proteasomal structure. This model helps to better understand the observed properties of the 20S molecule, and sets foundations for further studies of the structural dynamics of the proteasome.

The proteasome, a giant proteolytic assembly, plays a unique role among proteases (*1*). The enzyme is often considered as a molecular machine with its own functional compartments and a modular structure. The eukaryotic proteasome is involved in a remarkable broad range of functions: from removal of damaged or no longer needed proteins to the precise temporal cleavage of cell cycle related proteins and transcription factors. The structure of the proteasome has been studied extensively by X-ray crystallography and electron microscopy (*2−5*). On the other hand, our understanding of the catalytic mechanism and regulation of the elaborate structure is seriously lagging behind (*1, 2*).

The 20S particle resembles a hollow cylinder, or barrel, with a diameter of 11−12 nm, a length of 14−17 nm, and an approximate molecular mass of 700 kDa. The assembly is built from four stacked rings containing seven subunits in each ring (*2*). The two internal β-rings harbor the catalytic β-subunits with active centers facing inside of the 20S barrel. The β-rings are flanked by two α-rings composed of subunits devoid of active centers, but playing structural functions. The archaebacterial 20S proteasome is built from multiple copies of only one type of α- and one type of β-subunit, whereas the eukaryotic particle contains several distinct, but structurally related, α- and β-polypeptides. The 20S core particle degrades only peptides and unfolded proteins. Attachment of a 19S regulatory complex ("a cap") to the α-rings on both sides of the core particle leads to formation of the 26S proteasome, which also recognizes and cleaves ubiquitinated proteins. Proteasomes isolated from such diverse organisms as *Thermoplasma acidophilum*, fruit fly, clawed frog, and rat show a very similar structure when examined with an electron microscope (*3*). The crystal structures of the 20S particles isolated from two organisms, *T. acidophilum* and *Saccharomyces cerevisiae*, have been determined (*4, 5*). The general architecture of both proteasomes follows familiar properties with one exception. The α-rings of the archaebacterial proteasome are open, leaving a clear path to the catalytic chamber for potential substrates. Unexpectedly, the path is closed by the polypeptide chains of the α-subunits in the *S. cerevisiae* proteasome crystallized with inhibitors (*5*). It was postulated either that the hypothetical open conformation was not captured in the crystal (*1*), that the 19S cap is required to open the α-rings, or that substrates enter the catalytic chamber through the narrow side windows between the rings (*5*). To investigate these possibilities, we decided to use AFM to test whether the open conformation could be detected in the native 20S proteasome (*6*).

The tapping-mode atomic force microscopy (AFM) in liquid provides dynamic structural information on large biomacromolecular assemblies (*7−10*). Briefly, in this method, a small and very sharp vibrating tip is placed in close proximity to the sample so that it interacts with the object's atoms by van der Waals forces. These interactions change the resonant frequency or vibrational amplitude of

* Address correspondence to this author at the Institute of Biotechnology, University of Texas Health Science Center at San Antonio, 15355 Lambda Dr., San Antonio, TX 78245. Tel: (210) 567-7262; Fax: (210) 567-7269; E-mail: gaczynska@uthscsa.edu.

the tip. Such changes are monitored by the detection system and used as a measure of differences in the force gradient, which in turn reflects alterations in the tip-to-sample spacing, or sample topography. This nanoenzymological method is noninvasive, does not require protein fixation, can be performed in aqueous buffer at neutral pH, and allows for the repeated scanning and analysis of the same molecule under a wide range of conditions. Therefore, we took advantage of the AFM technique to observe and analyze native 20S proteasomes in action. As we have shown recently, the fission yeast proteasomes imaged in time lapse sequence by AFM repeatedly change their conformation between the state of open and closed α-rings. The preferred conformation depends on the ligands present. The control proteasomes in a buffer, the inhibited proteasomes, or proteasomes incubated with a nondegradable peptide remain closed most of the time. Addition of a model peptide substrate to the uninhibited enzyme shifts the equilibrium toward the open conformation (*6*). The existence of the open conformation has been subsequently confirmed by X-ray crystallography of mutant yeast proteasomes and of hybrid assemblies of yeast 20S proteasome with the activator complex from *Trypanosoma* (*11*, *12*).

The analysis of the top-view particles proved to be instrumental in addressing the problem of the "closed entrance" to the proteasome. In top-view particles, however, we were able to observe only the apical parts of α-rings. Here, we present a comprehensive study of the molecules in the side-view position, with both α- and β-rings available for imaging. Analysis of the proteasomes in this alignment allowed us to distinguish two stable allosteric conformations of the 20S particle and propose a molecular mechanism governing their formation and stability.

EXPERIMENTAL PROCEDURES

Purification of 20S Proteasome. The 20S proteasome was isolated from an exponentially growing culture of fission yeast *Schizosaccharomyces pombe* strain 972h⁻ and purified as described previously (*13*, *14*). Electrophoretically pure proteasomes were stored at −20 °C in 50 mM Tris/HCl buffer, pH 7.0, with 20% glycerol. The sample diluted with 5 mM Tris/HCl buffer, pH 6.8 (without glycerol), displayed proteolytic activity against the three commonly used fluorogenic peptide substrates: succinyl-LeuLeuValTyr-7-amino-4-methylcoumarin (SucLLVY-MCA), butoxycarbonyl-Leu-ArgArg-MCA (BocLRR-MCA), and carbobenzoxy-Leu-LeuGlu-β-naphthylamide (Z-LLE-βNA) (*13*). No degradation of fluorogenic peptides with unblocked N-termini, LVY-MCA and AAF-MCA was detected. All fluorogenic peptides were used at final concentrations of 100 μM. Commonly used inhibitors of the proteasome: lactacystin (40 μM), carbobenzoxy-LeuLeuLeuCHO (Z-LLL-CHO; 100 μM), and carbobenzoxy-LeuLeuLeu vinyl sulfone (Z-LLL-VS; 100 μM; all from Calbiochem), inhibited degradation of Suc-LLVY-MCA by at least 98%.

Imaging with Atomic Force Microscopy (*AFM*). For the AFM imaging, 2 μL of the sample diluted in 5 mM Tris/HCl buffer, pH 6.8, was deposited on a freshly cleaved mica surface, after a few minutes overlaid with 50 μL of the buffer used for dilution, and mounted in the "wet chamber" of the

NanoScope IIIa (Digital Instruments) (*6*). The imaging was performed in a tapping mode using oxide-sharpened silicon nitride tips on cantilevers with a nominal spring constant 0.32 N/m (Nanoprobe). The resonant frequency of the tip was tuned to 8−10 kHz, with an amplitude 200−600 mV and a setpoint of about 2 V. Areas ranging from 200 nm × 200 nm to 1.0 μm × 1 μm were continuously scanned with a rate of 2.1 Hz, and images were acquired with 512 × 512 pixels. Even with the observed lateral drift of about 10 nm per scan, it was still possible to observe the same group of molecules for an hour or longer. Peptide substrates (final concentration: 100 μM) or the inhibitors (40 or 100 μM) were injected directly into the chamber. This arrangement enabled imaging the same molecules before (control) and after addition of the ligands. All experiments were repeated at least twice. Stock solutions of peptides and inhibitors were made with dimethyl sulfoxide (DMSO), and the final concentration of the solvent reached 2% in the sample. Addition of DMSO without any ligand (23 side-view particles were analyzed) did not induce detectable changes in the proteasomes' conformation, as compared with the sample without DMSO. Also, no detectable changes in the distribution of conformers (30 particles were analyzed) described below were found when the ionic strength of the solution in the chamber was increased by addition of up to 200 mM NaCl in 20 mM Tris/HCl buffer (pH 7.0) (*6*, *15*). A standard plane fit provided in the NanoScope IIIa software was the only processing procedure applied to the images of the whole fields in the height mode. Brightness and contrast of the zoomed-in images were adjusted in Adobe Photoshop v. 5.5 software (Adobe Systems Inc.). Measurements of the particles were carried out with the section analysis software (Digital Instruments). The length of the molecule (frontal section) and its width (transverse sections) were measured 1 nm from the topmost point of the particle (see Figure 2b). The reported dimensions of particles were corrected for the tip convolution effect. This part of the analysis was performed on a Macintosh G4 computer using the public domain Image SXM v. 1.67-3P software (S. Barrett, Surface Science Research Center, University of Liverpool, Liverpool, United Kingdom), a version of the public domain image analysis software NIH Image (developed at the U.S. National Institutes of Health and available on the Internet at http://rsb.info.nih.gov/nih-image/). Specifically, an Image SXM function "tip locus effect" was utilized to calculate a map of the "locus" of the closest vertical interaction between the probe and the surface compensating for broadening caused by curvature of a parabolic finite-radius tip. The actual radius of curvature for every tip used was approximated from the image of calibration grating (Ultrasharp TGT01 silicon calibration grating, K-Tek International, Inc.), and usually was between 5 and 15 nm. The dimensions corrected for the tip convolution effect were smaller from the lengths and widths measured in raw images by about 10% for tips with 5 nm radius of curvature, and by about 30% for tips with 15 nm radius. Typically, 90−100% of all imaged particles recognizable as "side-view" by their shape, height, and shape of their cross-sections were measured in at least five scanned fields and included in the analysis. The only particles not included in the analysis (less than 10%) were clearly misshaped by thermal or mechanical noise. Normality of distribution of measurements was evaluated with the Sha-
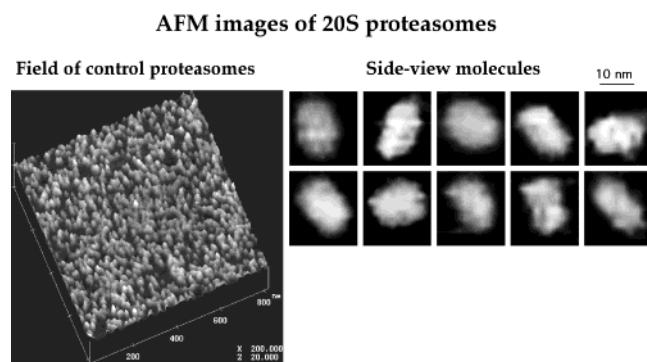
FIGURE 1: Molecules of native 20S proteasome imaged with tapping-mode AFM in liquid. The 20S proteasome was purified from fission yeast. (Left) Surface plot image of 800 nm × 800 nm field of densely packed proteasomes. The majority of particles are in a side-view position, with only a few "high standing cones" in the top-view position visible. The horizontal scale bar is X = 200 nm; the vertical scale (Z = 20 nm) is color-coded from black (height = 0) to white (20 nm). (Right) Array of enlarged images of the side-view molecules is presented. Note the variations in shape of the particles. The images of molecules were not averaged or filtered, besides interpolation automatically applied by the Nano-Scope software during imaging. Plane fit of the whole fields and brightness/contrast adjustment were the only processing steps applied to the images in this figure and in Figures 2 and 4.

piro−Wilk test (*16*). The data that did not follow the normal distribution were tested whether they consisted of more than one class of data using the centroid method of cluster analysis (*17*). In this method, similarity between clusters of data is measured as a distance between cluster centroids, or mean values of the objects contained in a cluster on a variable. When two clusters are combined, a new centroid is computed (*17*). This approach was used to separate the side-view molecules into the barrel-like and cylinder-like conformers.

RESULTS

We observed with AFM a field of randomly distributed 20S proteasomes on a surface of mica using our previously established conditions for the preparation of the protein samples and collection of images (*6*). Typically, we found from several to more than a hundred particles in a scanned field of 200 × 200 nm to 1 × 1 μm, respectively. We identified the molecules either as top-view or as side-view proteasomes on the basis of their distinctive shape and dimensions: they resembled either "standing" cones or "lying" cylinders. After applying the correction for the tip broadening effect (details under Experimental Procedures), the length of the side-view cylinders ranged from 14 to 17 nm, and their diameter measured at the midpoint of their length extended from 9 to 12 nm. The height of side-view particles measured from the edge of closely packed patches was 8−11 nm, in contrast to the 14−16 nm height of top-view particles. The obtained dimensions of the *S. pombe* proteasomes were consistent with the crystallographic (*5*), electron microscopy (*18*), and AFM data (*19*) collected with the *S. cerevisiae* complexes. At least half of the molecules were classified as side-view proteasomes. In agreement with the desired random distribution of the particles, the longi-tudinal axes of the side-view proteasomes pointed at different directions (Figure 1). Moreover, the distribution and dimen-sions of molecules did not depend on the size of the scanned fields.
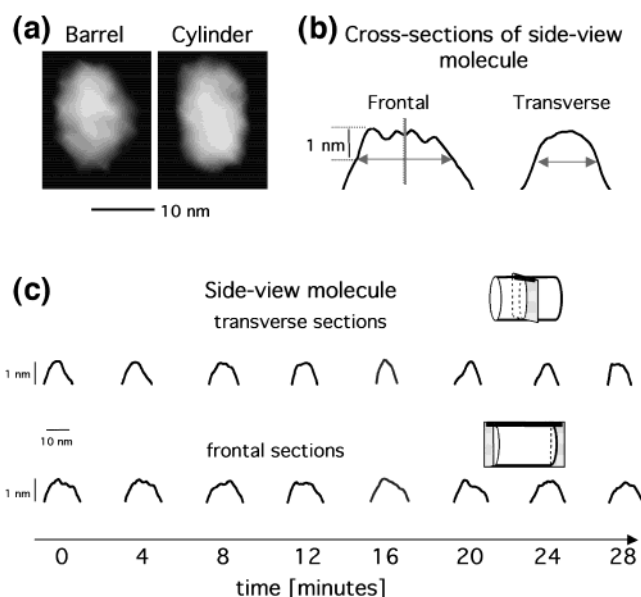

FIGURE 2: Side-view proteasome molecules acquire two conforma-tions: barrel-like or cylinder-like: (a) barrel- (left) and cylinder-like (right) control molecules; (b) cross sections of the control barrel proteasome. The length of the molecules (frontal section) and their width (transverse sections) were measured 1 nm from the topmost point of the particle as indicated by arrows. The dotted line marks the position of the transverse section. The diameter of the molecules was then calculated based on the width measurements. The reported dimensions of particles were corrected for the tip convolution effect (details under Experimental Procedures). (c) Cross sections of a control side-view particle imaged every 4 min. Only barrel form was detected except for the 16 min time point. Upper panel: transverse sections in the middle of the long axis of the molecule. Lower panel: frontal sections through the middle of the molecule, parallel to its long axis. The darker area of shading in the diagram corresponds to the part of the molecule represented by the sections.

Closer examination of the side-view complexes revealed the presence of two major populations of apparently distinct molecules. One class of molecules consisted of barrel-shaped proteasomes: they were relatively short but wide in the middle. The second class included relatively long, cylinder-shaped proteasomes (Figure 2). We found that the observed differences between these two classes of particles could be quantitatively expressed with a ratio of the length of the molecule to a diameter measured at the midpoint of the length of the same molecule (l/d, Figure 2b,c). Although values of the l/d parameter changed smoothly, we noticed that the frequency histogram of l/d values for the control particles did not follow the normal distribution (Figure 3). Cluster analysis executed with the centroid method (*17*) proved that there are two populations of the side-view molecules. Therefore, using the l/d parameter, we could reliably separate all the control molecules into two classes of "barrel-like" complexes with a small l/d ratio and "cylinder-like" com-plexes with a larger l/d ratio (Figure 3, Table 1). The cutoff point for separation of barrels from cylinders according to their l/d ratio was determined after analysis of the crossing points of theoretical normal distributions of the two classes of particles, found with the help of cluster analysis. The bell-shaped theoretical normal distributions of the two classes of particles crossed at the values l/d = 1.6 for the control set of data and at l/d = 1.5 for the set of data obtained after addition of a substrate to the proteasomes (Figure 3). Cluster analysis for all other sets of data (not shown) gave the
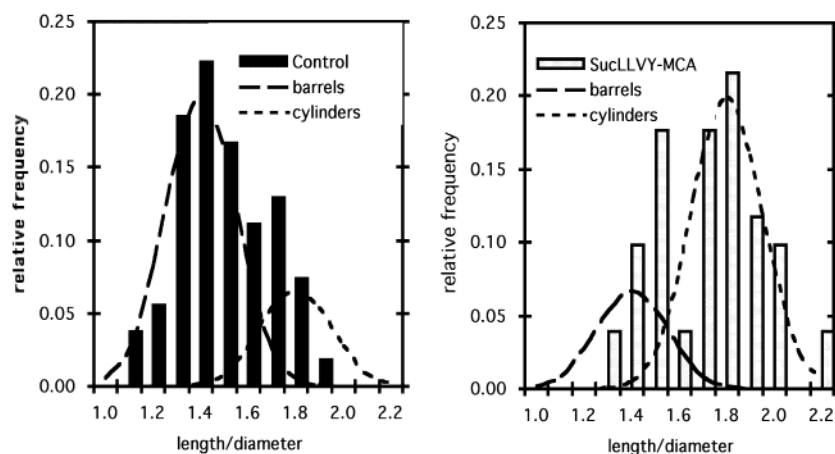
FIGURE 3: Frequency histograms of distribution of the length-to-diameter (*l/d*) ratios for the control proteasomes and proteasomes incubated with a substrate, SucLLVY-MCA. Dashed lines represent theoretical normal distributions of the barrel-like and cylinder-like classes of particles. The length and diameter of particles were measured as shown in Figure 2b.

Table 1: 20S Proteasomes in the Side-View Position Acquire Two Distinct Conformations: Barrel-like and Cylinder-like[a]

	control		+SucLLVY-MCA		+BocLRR-MCA		+Z-LLE-βNA		SucLLVY-MCA removed[b]	
	barrels	cylinders	barrels	cylinders	barrels	cylinders	barrels	cylinders	barrels	cylinders
length/diameter (*l/d*)	1.4 ± 0.1	1.8 ± 0.1	1.4 ± 0.1	1.7 ± 0.2	1.4 ± 0.1	1.8 ± 0.3	1.4 ± 0.1	1.7 ± 0.2	1.3 ± 0.1	1.7 ± 0.1
length (*l*)	15.1 ± 1.4	16.1 ± 0.9	15.2 ± 1.2	16.2 ± 1.8	15.6 ± 2.2	15.6 ± 2.2	14.6 ± 0.6	15.6 ± 2.2	15.8 ± 0.8	15.3 ± 0.9
diameter (*d*)	10.9 ± 1.3	9.2 ± 0.6	10.9 ± 1.0	9.7 ± 0.9	11.3 ± 1.4	8.8 ± 1.4	10.2 ± 0.5	9.1 ± 1.5	12.0 ± 0.9	9.3 ± 0.6
% of forms	76	24	27	73	24	76	27	73	74	26
n	90	28	11	30	8	21	6	17	23	8

	+LVY-MCA		+LC		+SucLLVY-MCA, +LC[b]		+Z-LLL-VS		+Z-LLL-CHO	
	barrels	cylinders	barrels	cylinders	barrels	cylinders	barrels	cylinders	barrels	cylinders
length/diameter (*l/d*)	1.4 ± 0.2	1.8 ± 0.1	1.4 ± 0.1	1.8 ± 0.1	1.3 ± 0.1	1.7 ± 0.1	1.4 ± 0.1	1.7 ± 0.1	1.4 ± 0.1	1.9 ± 0.1
length (*l*)	15.2 ± 0.8	15.6 ± 1.0	14.8 ± 2.0	15.7 ± 1.5	15.0 ± 1.6	15.6 ± 1.8	14.9 ± 0.9	15.1 ± 0.7	15.0 ± 1.5	15.3 ± 1.3
diameter (*d*)	10.5 ± 1.3	8.6 ± 0.6	10.3 ± 1.3	8.9 ± 1.0	11.3 ± 1.1	9.4 ± 1.1	11.0 ± 1.2	9.0 ± 0.7	10.5 ± 1.1	8.3 ± 1.6
% of forms	63	37	66	34	79	21	79	21	78	22
n	19	11	21	11	31	8	21	6	15	4

[a] All dimensions are given in nanometers and presented as mean ± SD for *n* particles. The control particles were sorted into barrel- and cylinder-like classes (see Experimental Procedures and Figure 3). Subsequently, molecules from all other experiments were measured (Figure 2b) and classified following the same routine. There were no statistically significant differences between particles belonging to the same class. The table shows the results of measurements of molecules in all experiments, control and with ligands. The *l/d* ratio was calculated separately for each molecule, and then the means and SDs were calculated from the set of ratios, all single *l/d* values representing single molecules. The *l/d* ratio differed significantly between barrels and cylinders. All measured and calculated parameters, as well as the distribution of the two conformers, were undistinguishable between control particles and particles imaged under high ionic strength conditions (0.1−0.2 M NaCl; *n* = 20 analyzed particles; 25% of cylinders) or between control (nonligated) particles imaged with the highest and lowest pixel size of the image (scanned fields of 200 nm × 200 nm or 1 μm × 1 μm, with *n* = 30 and *n* = 70 analyzed particles; 30% and 24% of cylinders, respectively). [b] These columns illustrate reversibility of the shift of the equilibrium between barrel-like and cylinder-like molecules in accord with our model (Figures 5 and 6).

crossing points always in the range between 1.5 and 1.6 of *l/d* values, and these values were used as cutoff points for the respective sets of data. For a maximum objectivity, we strictly followed this mathematical method for separation of conformers. Interestingly, the barrel conformation comprised about 76% of the side-view control molecules.

Similarly to the top-view molecules, the same side-view particles scanned repeatedly were not locked in one conformation but acquired either conformation, with the barrel shape prevailing (Figures 2c and 4). However, the mode of data collection did not permit us to detect any periodicity of the switch between the conformers.

Previously, we showed that treatment of the proteasomes with model peptide substrates shifted the equilibrium of the top-view particles toward molecules with the open α-rings (6). However, the addition of either noncleavable peptides

or proteasomal inhibitors preserved the control-like preference for molecules with the closed α-rings. Here, we extended our study to test if these ligands would affect the conformation of side-view molecules. After the addition of SucLLVY-MCA, the model substrate of proteasomal chymotrypsin-like activity, both the barrel and cylinder conformations were still clearly distinguishable, though this time the particles preferably took the shape of a cylinder (73%; Figure 4). Virtually identical results were obtained with other model substrates: BocLRR-MCA (trypsin-like activity) and Z-LLE-βNA (PGPH, or postglutamyl peptide hydrolyzing activity). In contrast, when LVY-MCA, the peptide that is noncleavable by the proteasome, was added, the barrel-like particles were in the majority, resembling the distribution of the molecules in the control samples (Table 1). On this basis, we speculated that the stabilization of the specific side-
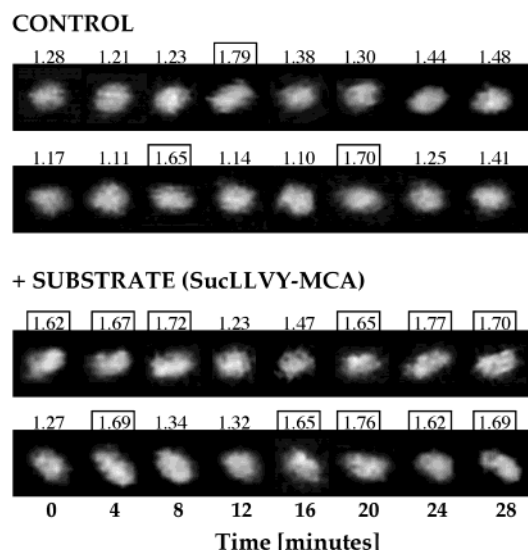
FIGURE 4: All the imaged 20S molecules switched their conformations; however, the relative content of the cylindrical molecules increased upon addition of the substrate. The dimensions of four typical molecules in the side-view position were measured after imaging them in 4 min intervals and were corrected for the tip convolution effect as described under Experimental Procedures. Every row of images represents a single analyzed particle, with its l/d ratio posted above the corresponding image. The particles were of the barrel- or cylinder-like shapes. The classification of single molecules into the particular class was performed according to their l/d ratio. The cutoff value of the l/d ratio was calculated from the theoretical normal distributions of the two classes of particles. The particles classified as cylinder-like have their l/d ratios enclosed in rectangles.

view conformers was controlled either by simultaneous occupancy of the binding site and active center or by occupancy of the active center alone.

To distinguish between these possibilities, we tested whether blocking the active centers with the specific proteasome inhibitors, lactacystin, Z-LLL-VS, and Z-LLL-CHO, would affect the conformation of the 20S complexes. All three inhibitors bind covalently to the active site threonines inside the β-rings. Lactacystin and Z-LLL-VS bind irreversibly, whereas binding of the tripeptide aldehyde is reversible (*20*). Both the tripeptide derivatives closely resemble the polypeptide substrates of the proteasome. These two inhibitors presumably bind both to the active centers and to the binding sites inside the catalytic chamber. Lactacystin, on the other hand, binds only to the active site threonines (*20*). Analysis of the side-view molecules treated with the inhibitors revealed the presence of both conformers; however, the barrel-like particles were predominant (Table 1).

Finally, we tested whether the observed distribution of the top- and side-view conformers was reversible. Specifically, we tested whether the open and cylinder-like conformers are still fully capable to revert to the "mostly closed" and "mostly barrel-like" populations. To address this question, we analyzed images of the randomly distributed proteasomes in the following order. First, we collected the images of the untreated, control molecules. Subsequently, SucLLVY-MCA peptide substrate was added, and images were collected again. Then the substrate was removed with several washes with the Tris/HCl buffer, and images were collected several times. Alternatively, the substrate-treated sample was additionally treated with the irreversible inhibitor lactacystin.
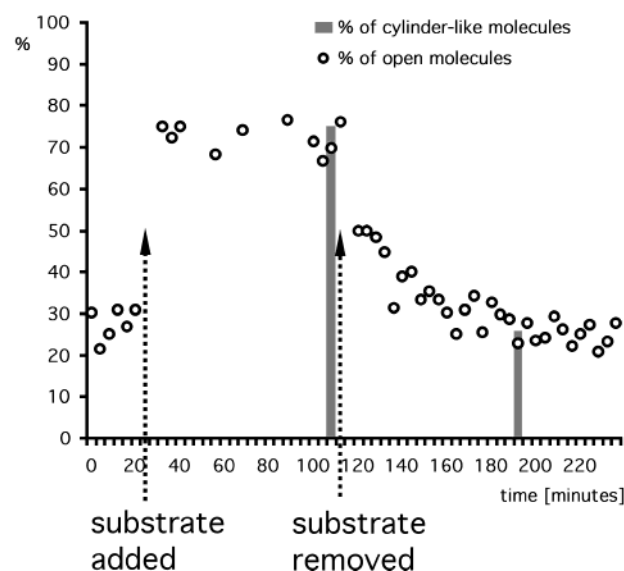

FIGURE 5: Closed−open and barrel−cylinder conformational transitions are reversible. The field of proteasomes was scanned continuously, with one scan lasting 4 min. After 24 min, the substrate SucLLVY-MCA was added to the sample, and the field was scanned for over an hour. Then, the sample was washed 5 times with 100 μL of 5 mM Tris/HCl buffer. The scanning resumed after 8 min of washing and proceeded for nearly 2 h. Control top-view proteasomes contained 28% $\pm$ 4% of open molecules ($n = 6$ fields with 145 particles); after addition of the substrate, the content of open molecules shifted to 74% $\pm$ 3% ($n = 10$ fields with 183 particles). After removal of the substrate, the content of open molecules decreased gradually and reached 26% $\pm$ 3% in 16 fields (176 min in the last scan). The content of cylinder-like side-view molecules reached 75% in fields scanned between 100 and 112 min (20 particles), and fell to 26% between 188 and 200 min. (31 particles). In another experiment performed to test the reversibility of the transition, the 20S proteasomes were adsorbed on mica without any ligand added, and the conformers were counted as described. Subsequently, SucLLVY-MCA substrate was added, and after 10 min incubation, the conformers were counted again. Finally, lactacystin (LC) was added, and after another 10 min incubation, the conformers were counted (Table 1). Percent of cylinder-like molecules after addition of LC fell to 21 (8 fields, 39 particles). In this experiment, we obtained the following percentages of open top-view molecules: for the control, 23 $\pm$ 3 ($n = 7$ fields; 130 particles); after addition of SucLLVY-MCA, 73 $\pm$ 2 ($n = 7$; 100); and after addition of LC, 23 $\pm$ 3 ($n = 8$; 140).

Examination of the images indicated that the shifts of the open−closed and the barrel−cylinder molecule's equilibria were fully reversible if only the reaction with the ligand used was reversible (Table 1, Figure 5).

DISCUSSION

The work presented here shows that the 20S proteasome molecules observed with AFM under native conditions constantly alternate their global architecture, switching between several distinct conformations. In our previous work, we discussed the diversity of the top-view molecules (*6*). Here, we distinguished two types of discrete conformants among the side-view particles. They were classified as either barrel- or cylinder-shaped molecules. We noticed that the relative abundance of the conformers depended on the presence of a particular type of ligand.

The detection of the ligand-dependent shapes of the proteasomes leads to the question about properties of a macromolecule contributing to formation of the AFM image.

First, in the absence of nonspecific interactions between a tip and the object, it is the actual physical shape of the molecule. Nanometer-scale movements of domains or sub-units of the complex are the next most important factor. If the movements are slower than the temporal resolution of data collecting, it is possible to observe a set of molecules representing defined structural forms. At the same time, it is also possible to catalog distinct forms adopted by the same molecule during the subsequent scans. To ensure preservation of the same interactions between a sensing tip and the surface of the protein, we always compared molecules scanned under exactly the same physical conditions, changing only the ligands present. We established that altering the ionic strength of the buffer and thus varying the tip–protein interactions did not introduce any measurable changes in the appearance and distribution of the conformers. In addition, changing the size of the scanned field and the direction of scan did not affect our results (Table 1). These facts strongly support a notion that the detected conformational changes reflected the authentic properties of the proteasome molecules and they did not arise from methodological artifacts.

We found that the global architecture of the side-view molecules changed in nanometer-scale between barrel-like and cylinder-like shapes. In fact, the properties of the barrel–cylinder transition were similar to the already described open–closed transition (*6*). In both cases, the proteasomes stayed in one conformation for at least a few seconds, which is the time necessary to form an image of a single molecule. In addition, in both cases, the molecule switched quickly between the long-lived, most stable conformers. Similarly to the open and closed conformations, the large spatial amplitude and temporal extent of the detected protein movements clearly indicated allosteric transitions as their source (*21*).

Biochemical evidence points at the strong allostery between active centers on β-subunits, and active centers and hypothetical regulatory sites (*22, 23*). Since the polypeptide chains of the proteasomal subunits are tightly interwoven (*5*), it is reasonable to envision a transfer of structural changes between the rings. The long-distance transfer of structural changes postulated here is not unusual among the giant proteolytic complexes. For example, in the bacterial homo-logue of the proteasome HSlV protease, the conformational change caused by binding the HslU ATPase complex is transmitted to the active site region of the protease (*24*).

The detection of the closed and open top-view molecules, and the barrel and cylinder side-view molecules, raises the question as to whether these conformers represent the proteasomes in exactly the same state but just perpendicularly oriented on the mica. The distributions of the closed and open populations were in fact identical to the distributions of the barrels and cylinders in all the analyzed samples (Table 1, Figure 5) (*6*). Therefore, we postulate the presence of two key proteasome conformers grouped as the closed/barrel-like and open/cylinder-like molecules.

The existence of the two distinct but interconverting conformations suggested that they might represent allosteric states R and T of the enzyme in accord with the classical two-state model (*25*). Let us assume that the closed barrels correspond to the R form, and the open cylinders to the T form (Figure 6). At this point of our studies, we can reliably distinguish the R and T forms in all our AFM images, but
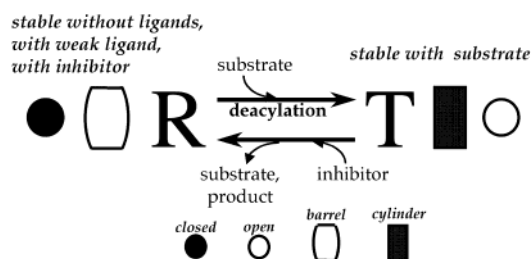

FIGURE 6: Proposed two-state model of allosteric transitions for the eukaryotic 20S proteasome. The top-view conformers are depicted as either empty or filled circles. The side-view conformers are represented by either regular or barrel-shaped rectangles. The R and T forms could be in either the ligated or the nonligated state. See the text for details.

we cannot determine if the conformers are ligated or nonligated. However, we can assume that there are two nonligated forms present in the control sample: R_0 and T_0. The form R_0 is thermodynamically more stable and hence-forth more abundant than the T_0 form. Therefore, we observed mostly the closed barrels in our control samples. Addition of the substrate creates two new ligated forms, R_L and T_L. In this case, the form T_L is more stable than R_L, showing its higher affinity for the ligand, what is reflected by the shift of the equilibrium toward the T_L form. Contrary to it, since LVY-MCA is a weak ligand, we observed the majority of the closed barrels (R_0) again. Lactacystin and Z-LLL-VS bind irreversibly to the active centers of the proteasome, but their addition fails to promote the T_L form (open cylinders), and instead the R_L form (closed barrels) is stabilized. Addition of the reversible competitive inhibitor Z-LLL-CHO results in a distribution of conformers similar to that observed with irreversible inhibitors. Apparently, only the substrates are capable of stabilizing the T, or open cylinder, form. The transitions between R and T forms are reversible, with the only restriction that the active centers are not blocked by the irreversible inhibitors (*6*). The stabilization of the T_L form in the presence of a substrate can be reversed by washing out the substrate or by blocking active centers with irreversible inhibitors, thus rendering the centers inaccessible for the substrate (Figure 5, Table 1).

Clearly, catalytic action is necessary for stabilization of the T_L form, since the particles remained open and cylinder-shaped for most of the time only when the substrate was added to the catalytically active (uninhibited) enzyme. Both the competitive inhibitors and the substrates acylate the active site threonines. Therefore, we exclude acylation as the step specifically promoting the T conformation. We hypothesized before that the deacylation step during amide bond cleavage promotes the open conformation (*6*). Therefore, we may generalize this finding, and hypothesize that expelling the N-terminal product, or expelling the C-terminal product, or the deacylation step in general, results in the shift in the equilibrium toward the T form (Figure 6).

At this stage of the study, our approach does not take into account the presence of the multiple active centers and binding sites, the influence of active centers on each other, and potential interactions of active centers with other structural elements of the proteasome. The work leading to distinguishing between the ligated and nonligated R and T conformers is in progress in our laboratory. We have to consider our model of allosteric regulation as only an

approximation of how the complicated machinery of proteasome works. Despite these limitations, the two-state model should be helpful in the evaluation of interactions between proteasomes and their ligands, especially inhibitors. This approach will also be instrumental for the better understanding of the molecular basis of elements globally controlling the enzymatic activity of the proteasome.

REFERENCES

1. Rock, K. L., and Goldberg, A. L. (1999) *Annu Rev. Immunol. 17*, 739−779.

2. Bochtler, M., Ditzel, L., Groll, M., Hartmann, C., and Huber, R. (1999) *Annu. Rev. Biophys. Biomol. Struct. 28*, 295−317.

3. Walz, J., Erdmann, A., Kania, M., Typke, D., Koster, A. J., and Baumeister, W. (1998) *J. Struct. Biol. 121*, 19−29.

4. Lowe, J., Stock, D., Jap, B., Zwickl, P., Baumeister, W., and Huber, R. (1995) *Science 268*, 533−539.

5. Groll, M., Ditzel, L., Lowe, J., Stock, D., Bochtler, M., Bartunik, H. D., et al. (1997) *Nature 386*, 463−471.

6. Osmulski, P. A., and Gaczynska, M. (2000) *J. Biol. Chem. 275*, 13171−13174.

7. Bustamante, C., Erie, D. A., and Keller, D. (1994) *Curr. Opin. Struct. Biol. 4*, 750−760.

8. Hansma, H. G., Kim, K. J., Laney, D. E., Garcia, R. A., Argaman, M., Allen, M. J., et al. (1997) *J. Struct. Biol. 119*, 99−108.

9. Engel, A., Lyubchenko, Y., and Muller, D. (1999) *Trends Cell Biol. 9*, 77−80.

10. Muller, D. J., Baumeister, W., and Engel, A. (1996) *J. Bacteriol. 178*, 3025−3030.

11. Groll, M., Bajorek, M., Kohler, A., Moroder, L., Rubin, D. M., Huber, R., et al. (2000) *Nat. Struct. Biol. 7*, 1062−1067.

12. Whitby, F. G., Masters E. I., Kramer, L., Knowlton, J. R., Yao, Y., Wang, C. C., et al. (2000) *Nature 408*, 115−120.

13. Gaczynska, M., Rock, K. L., and Goldberg, A. L. (1993) *Nature 365*, 264−267.

14. Osmulski, P. A., and Gaczynska, M. (1998) *Curr. Biol. 8*, 1023−1026.

15. Muller, D. J., Fotiadis, D., Scheuring, S., Muller, S. A., and Engel, A. (1999) *Biophys. J. 76*, 1101−1111.

16. Shapiro, S. S., and Wilk, M. B. (1965) *Biometrika 52*, 591−611.

17. McIntyre, R. M., and Blashfield, R. K. (1980) *Mult. Behav. Res. 15*, 225−238.

18. Coux, O., Tanaka, K., and Goldberg, A. L. (1996) *Annu. Rev. Biochem. 65*, 801−847.

19. Dorn, I. T., Eschrich, R., Seemuller, E., Guckenberger, R., and Tampe, R. (1999) *J. Mol. Biol. 288*, 1027−1036.

20. Bogyo, M., McMaster, J. S., Gaczynska, M., Tortorella, D., Goldberg, A. L., and Ploegh, H. (1997) *Proc. Natl. Acad. Sci. U.S.A. 94*, 6629−6634.

21. McCammon, J. A., and Harvey, S. C. (1987) in *Dynamics of proteins and nucleic acids*, pp 28−30, Cambridge University Press, Cambridge U.K.

22. Kisselev, A. F., Akopian, T. N., Castilio, V., and Goldberg, A. L. (1999) *Mol. Cell 4*, 395−402.

23. Myung, J., Bo Kim, K., Lindsten, K., Dantuma, N. P., and Crews, C. M. (2001) *Mol Cell 7*, 411−420.

24. Sousa, M. C., Trame, C. B., Tsuruta, H., Wilbanks, S. M., Reddy, V. S., and McKay, D. B. (2000) *Cell 103*, 633−643.

25. Monod, J., Wyman, J., and Changeux, J. P. (1965) *J. Mol. Biol. 12*, 88−118.